

3D PHASE CORRELATION USING NON-UNIFORM CYLINDRICAL SAMPLING

Jakub Bican and Jan Flusser

*Institute of Information Theory and Automation, Pod vodárenskou věží 4, 18208 Prague 8, Czech Republic
Faculty of Mathematics and Physics, Charles University in Prague, Ke Karlovu 3, 121 16 Prague 2, Czech Republic*

Keywords: Image registration, Phase correlation, Cylindrical transform, Rigid-body transform, Experiments.

Abstract: A Phase Correlation Method (PCM) is a well known and effective strategy for 2D image registration. Earlier we presented a derived method called Cylindrical Phase Correlation Method (CPCM) which belongs among many improvements and applications of PCM published by other authors. CPCM utilizes the effective and robust approach of PCM for a 3D image rigid registration task in an iterative optimization procedure. In this paper, the improvement to the rotation estimation step based on the non-uniform sampling in the cylindrical coordinate system is described in detail. Experimental results are provided both for the original and improved version of the rotation estimation algorithm as well as the results of the final method and its comparison to reference methods.

1 INTRODUCTION

Rigid body registration task is a very important area in the space of image registration methods (Zitová and Flusser, 2003). The purpose of rigid body registration algorithms is to spatially align a pair of images mutually rotated and translated. This is often a case in medical image registration: the images of rigid parts of human body (especially head) taken at different times are aligned to detect the changes across the time.

The presented method – Cylindrical Phase Correlation (CPCM) introduced in (Bican and Flusser, 2007) – is a 3D rigid body registration algorithm that fits into a family of optimization methods that aim to find an extreme of similarity or dissimilarity measure on a multidimensional space of parameters of a selected transform model by some numerical optimization process (Zitová and Flusser, 2003). CPCM is based on a Phase Correlation Method (PCM) first introduced by (Kuglin and Hines, 1975) as a fast and robust method for estimation of inter-image shifts. PCM was extended by (De Castro and Morandi, 1987) to register translated and rotated images and later by (Reddy and Chatterji, 1996) to register translated, rotated and scaled images. All of the referenced approaches process 2D images, while (Keller et al., 2006) introduced an algorithm for the registration of rotated and translated 3D volumes based on

Pseudopolar Fourier transform. Their approach uses the pseudopolar representation of spectral magnitudes to find the rotation axis and estimate the rotation angle without using interpolation. More details to the background of CPCM can be found in (Bican and Flusser, 2007).

In this paper, we describe in detail the rotation estimation improvement first laid out in (Bican and Flusser, 2007). The improvement is based on the non-uniform sampling in the cylindrical coordinate space and therefore reduces the non-uniformity of the standard cylindrical approach with respect to the original orthogonal grid. We also provide an experimental examination of the improvement.

2 METHOD OVERVIEW

Rigid body transform is a transform that combines rotations and translations. Finding optimal parameters of rigid body transform (six parameters in 3D) is a very usual task of image registration (Zitová and Flusser, 2003) (intra-subject studies, multimodal registration, etc). As it was mentioned in the introduction, there is a class of registration methods that employ a numerical optimization process to find the optimum of similarity measure on a space of parameters of a transformation model. Our algorithm uses

below described procedures of *translation estimation* and *rotation estimation* to find parameters of rigid body transform so that the PCM metric – the correlation of whitened images – reaches its maximum. The optimization runs in iterations. Each iteration aims to improve the measure with respect to some subset of parameters. Such optimization resembles some well known optimizers – e.g. Powell’s direction set method (Press et al., 1992) – and is sometimes called *alternating optimization*.

The algorithm starts with identity transform T and a set of three linear independent axes (e.g. x , y and z). In each iteration, a transform update T_{upd} is computed and merged with actual transform: $T \leftarrow T \circ T_{\text{upd}}$. This iterative process is stopped if there was no non-zero update found in last six iterations (no transform parameter can be further optimized), or if the maximum number of iterations is met (time limit) or if the actual result is good enough (e.g. algorithm is stopped by an operator).

2.1 Odd Iterations: Translation Estimation

The translation estimation steps are based clearly on Phase correlation method by (Kuglin and Hines, 1975). PCM takes advantage of *Fourier shift theorem* that relates the phase information of spectrums of a reference image f_R and its shifted copy. If moving image f_M is the shifted copy of f_R then the inverse Fourier transform of so-called *cross-power spectrum* forms a correlation surface corr – i.e. a correlation value (of whitened images) for all possible discrete shifts:

$$\text{corr}(\tilde{\omega}) = \mathfrak{F}^{-1} \left(\frac{F_M F_R^*}{|F_M| |F_R|} \right) . \quad (1)$$

Thus, locating a peak in a correlation surface corr results in offset $\Delta \vec{x}$ that can be used to align f_R and f_M at pixel level:

$$\begin{aligned} \text{PCM}(f_R, f_M) &= \Delta \vec{x} = \text{argmax}_{\vec{x}} (\text{corr}(\vec{x})) , \\ T_{\text{upd}} &\leftarrow \text{PCM}(f_R, T(f_M)) . \end{aligned} \quad (2)$$

2.2 Even Iterations: Rotation Estimation

In 2D, the rotations around a fixed centre may be estimated by the PCM method executed on polar-transformed images (De Castro and Morandi, 1987). In the same way how polar transform converts rotations to translations in 2D, the cylindrical transform may be used to convert rotation around fixed axis to a translation in 3D.

Let’s represent the rotation by axis \vec{v} and angle α and assume that the rotation axis \vec{v} is known. For simplicity suppose, that the rotation axis is the z axis of the Cartesian coordinate system. Transformation to cylindrical coordinates about z axis is computed as $f^{*z}(\alpha, r, z) = f(r \cos \alpha, r \sin \alpha, z)$. Rotation of image f_R by angle $\Delta \alpha$ has the same effect as shifting the periodically extended image f^{*z} by $\Delta \vec{x}^{*z} = (\Delta \alpha, 0, 0)$

$$\begin{aligned} f_M(\vec{x}) &= f_R(R_z(\Delta \alpha) \vec{x}) , \\ f_M^{*z}(\vec{x}^{*z}) &= f_R^{*z} \left((\vec{x}^{*z} + \Delta \vec{x}^{*z}) \bmod S_{f_R^{*z}} \right) , \end{aligned} \quad (3)$$

where $R_z(\Delta \alpha)$ is the rotation matrix for rotation about z axis (Baker, 2007) and $S_{f_R^{*z}}$ is the size of image f_R^{*z} . (Asterisk superscript $(^{*z})$ denotes here the cylindrical coordinate system with axis z .)

Now it is clear that the rotation angle $\Delta \alpha$ can be estimated by PCM on cylindrically transformed images f_R^* and f_M^* :

$$T_{\text{upd}} \leftarrow \text{PCM}(f_R^{*z}, T(f_M^{*z})) . \quad (4)$$

Axes cyclically alternate as the algorithm advances so that for example in iterations 2, 4, 6, 8, 10... are used axes x, y, z, x, y, \dots respectively.

3 ROTATION ESTIMATION IMPROVEMENT

The approach described in previous section has two main drawbacks. The first one is caused by performing computations in discrete domain: when making cylindrical transform of the images, it is necessary to use higher order interpolation, because the cylindrical transform (alike a polar transform) is sampling the space very non-uniformly.

The second drawback is that the voxels of original volume located near the axis of the cylinder have much greater impact than the voxels located at the perimeter. If the angular and radial coordinate is sampled so that the perimeter of the cylinder is not subsampled and no information is lost, every voxel near the axis is stretched (or interpolated) to several voxels, while the voxels at the perimeter are resampled approximately one-to-one. Moreover, the PCM gives the same significance to well sampled voxels at the perimeter as to resampled voxels originating from the voxels near the axis, which are also highly affected by interpolation error.

These drawbacks led us to develop technique which computes PCM separately for every *layer* of the cylinder defined by fixed radius. Every such layer has different angular resolution that suitably samples

the original data: layer at radius r is in angular direction sampled by $2\pi r$ samples, i.e. with resolution (spacing) $2\pi/2\pi r = 1/r$ radians.

$$I_R^r(\alpha, z) = f_R^*(\alpha, r, z) \quad \forall \alpha = 0, 1/r, \dots, (2\pi - 1)/r \\ \forall z = 0, 1, \dots, S_{f_R}^z \quad (5)$$

Such sampling is a result of an effort to have the pixels approximately the same size in all layers and in the original orthogonal grid. The r value is determined as the spacing value in simple case (if the sampling of the original data is the same in each direction) or as the minimum (to preserve all data), maximum (to save memory resources), average or some other computed value of the spacings in all directions of the original data. Therefore the cylindrical pixels are r wide and r long. Figure 1 displays the sampling in the simple case. The maximum r may be also determined in different ways. In this paper, we use r as the half of the maximum size of the data across all dimensions, so we make an inner envelope in case the data have the same size in all dimensions, and therefore we use something between inner and outer envelope if this does not apply. In ideal case, the region-of-interest should be detected and included whole in the cylinder. Similar considerations apply also for the height of the cylinder z (we use $2r_{max}$).

Corresponding layers from reference and moving image are registered by PCM which results in a correlation surface that gives a degree of match for each angle. Correlation surfaces from all layers are then summed to get the global correlation surface

$$\text{corr}_{\text{imp}}(\alpha, z) = \sum_{r=1}^{S_{f_R}^r} r \mathfrak{F}^{-1} \left(\frac{L_R L_M^*}{|L_R| |L_M|} \right) (\alpha, z) , \quad (6)$$

where $L_{R|M}$ are Fourier transforms of layers $I_{R|M}$. Each layer is weighted by its radius r which corresponds to the number of pixels it contains. This gives to each original voxel same impact on the result.

Off-grid image values in equation (5) are computed using linear interpolation. Off-grid layer correlation surface values in equation (6) are computed using nearest-neighbour interpolation. Finally, position of the highest peak in the combined correlation surface corr_{imp} gives the final result of the registration

$$\text{IRE}(f_R, f_M) = \text{argmax}_{\alpha, z} (\text{corr}_{\text{imp}}(\alpha, z)) . \quad (7)$$

We call this algorithm *improved rotation estimation* and use it in the even iterations of CPCM to estimate the rotation. A comparison with basic version of the rotation estimation algorithm is shown in experimental part of the paper.

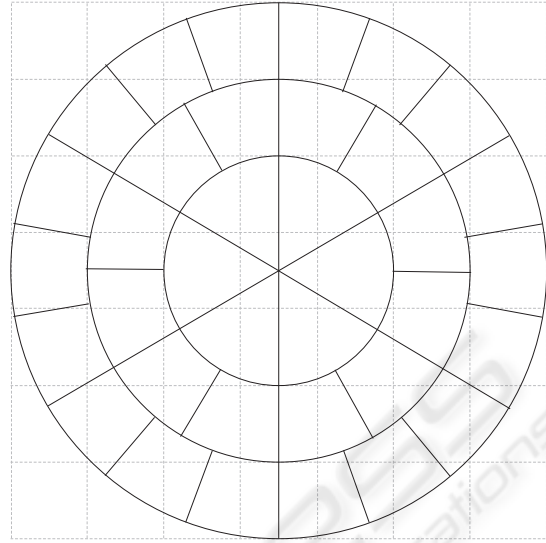


Figure 1: An example of the sampling approach in the improved version of the rotation estimation algorithm. Each layer of the cylinder is sampled with appropriate resolution. The first three layers of pixels of improved cylindrical sampling are displayed on top of regular orthogonal pixel grid.

4 EXPERIMENTAL RESULTS

In this section, we present outputs of some experiments that have been done to examine the performance of the CPCM method. First, the results of the whole method are reviewed, as they were published in (Bican and Flusser, 2007). Second, the improved version of the rotation estimation algorithm is examined and compared with the basic version.

In the experiments and results below, the sizes and distances are presented in millimetres as the usual medical volumetric data have different spacing (sampling, voxel size) in each dimension. To relate the presented distances with the voxel grid, see the caption of the appropriate figure presenting the data.

4.1 3D Rigid Registration Performance

In the first experiment, whole CPCM method including the improvement is examined. We use the method to register randomly rotated and shifted real MRI brain image (volume size is $128 \times 128 \times 40$ with $1.8 \times 1.8 \times 4.58$ mm spacing) with the original. The degree of misregistration as well as the registration error is measured by a fixed set of eight points that uniformly sample the reference image's volume. The error (or misregistration) is then measured as a mean Euclidean distance of these points in moving image to their original counterparts in reference image. This

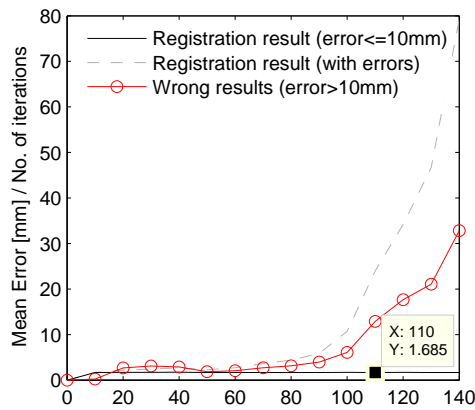


Figure 2: Influence of initial misregistration on the mean error after registration in successful registration cases and cases where the registration did not decrease the error under 10 mm level. Percentage of these failure cases is shown by the third series.

could be understood as a mean distance of every point of a volume to its transformed counterpart.

We continuously generated random transforms, so that there was *at least one hundred of different transforms for each 1 mm level of initial misregistration*. For each misregistration level, the results are the mean values over all transforms that introduced misregistration of that level. The graph in Fig. 2 shows two alternative views of the results. First, we filtered only those results that successfully converged under some *reasonable error* (here 10 mm – explained below). Then the graph also plots values that include all results. The figure also shows the statistics of failures, i.e. the percentage of cases when the method was not able to decrease under the error level 10 mm. The failure happens due to the local solution found during the optimization or due to the maximum number of iterations reached (the limit was 120 iterations).

The results can be interpreted such that until the misregistration is up to about 100 mm, the method converges to the pixel level precision with at least 90% reliability. As misregistration grows over 100 mm (which is approximately the radius of the volume), the failure rate increases and method's performance decreases mainly due to cases in which method converged to some false position. We should point out that these results and trends do not depend on the specific value of *reasonable error* mentioned above. We use value of 10 mm that is one order higher than the pixel size and is still reasonable small, but we could use values 5-45 mm without any significant effect on the graph.

4.2 Influence of Noise and Rotation Axis Error on Rotation Estimation

Algorithms for estimation of rotation angle (basic and improved version described above) were tested for robustness under non-ideal conditions. First, we want to examine the influence of these conditions on algorithm's behaviour and second, we want to justify the improvement.

In the first part of this experiment, a simulated MRI brain image (BrainWeb (Collins et al., 1998) simulated MRI brain image — volume size is $181 \times 217 \times 180$ with regular 1 mm spacing in all dimensions) was rotated around fixed axis by random angle and Gaussian noise was added to the rotated image. The rotation angle was then recovered by both basic and improved version of the algorithm and an absolute difference of estimated and original angle was measured as an estimation error. We generated many random angles for each level of noise with a new instance of noise for each measurement. Graph 3a shows averaged errors over all measurements for each level of noise.

The second part of this experiment was similar but instead of adding noise we shifted rotation axis in a random direction. Hence the algorithms were estimating rotation around different axis than the image was originally rotated (note that these algorithms may not recover original rotation axis). Graph 3b shows dependency of rotation angle error on the distance of the axis shift (again, error was averaged over many measurements for each shift distance).

Algorithms proved extreme robustness to noise. This can be explained due to averaging nature of PCM: we look for a single peak (ideally delta-function) in a correlation surface which is result of an inverse DFT of frequency spectra combined from the two images. The single peak is kind-of-average (linear combination) of all frequency samples that are affected by the same noise as spatial samples of original images. The variance of noise is reduced by averaging, hence thanks to large number of samples of 3D volume is the error of estimated rotation angle low even for really extreme noise.

If the rotation axis is shifted during rotation estimation, the algorithms were able to recover the angle as long as some structures in the data match. In both parts of the experiment, it is clearly observable positive effect of the improvements given in section 3. The effect of noise is reduced as well as the effect of disturbances between the two images (shifting the axis affects mainly the area near rotation axis which causes most problems in basic version of the algorithm).

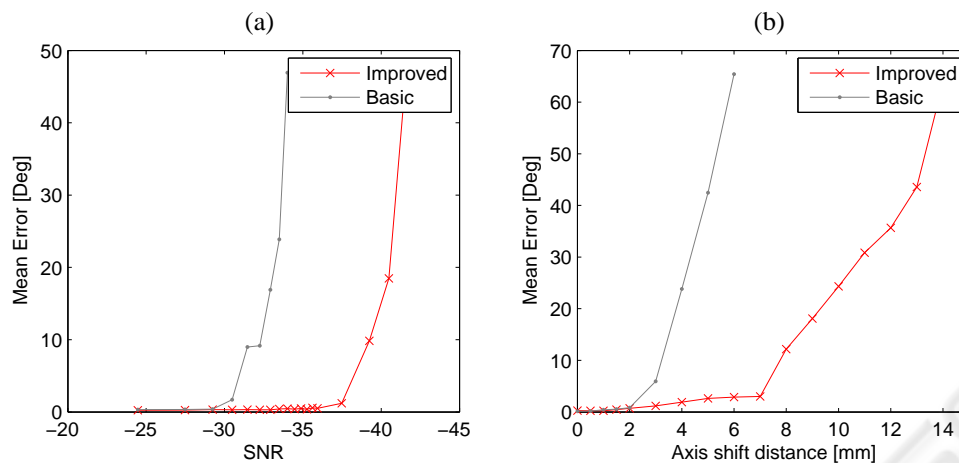


Figure 3: Influence of noise (a) and axis error (b) on rotation estimation.

5 CONCLUSIONS

We presented an image registration algorithm that is able to geometrically align mutually translated and rotated pair of 3D images. The method iteratively recovers translational component of misalignment by PCM and rotational component of misalignment by applying PCM on cylindrically mapped images. The improvement was given to the rotation estimation step to reduce the effect of noise and other image disturbances.

The experimental results show that the method is highly resistant to noise and image disturbances. This resistance is based on the presented improvement to the rotation estimation step.

Further improvements would focus on the precision of the method as the actual CPCM is able to register only with the pixel-level precision. We are also going to examine the multi-modal registration potential as the correlation of whitened images correlates mainly the image edges and therefore should be able to register images with common edges but different intensity levels.

ACKNOWLEDGEMENTS

The authors would like to thank to Czech Ministry of Education for support under the project No. 1M6798555601 (Research Center DAR) and to the Charles University in Prague for support under the project GAUK 48908 (Medical Image Registration and Fusion).

REFERENCES

- Baker, M. (1998-2007). www.euclideanspace.com: Maths - rotations.
- Bican, J. and Flusser, J. (2007). Cylindrical phase correlation method. In Kropatsch, W. G., Kampel, M., and Hanbury, A., editors, *Computer Analysis of Images and Patterns, 12th International Conference, CAIP 2007, Vienna, Austria, August 27-29, 2007, Proceedings*, volume 4673 of *Lecture Notes in Computer Science*, pages 751–758. Springer.
- Collins, D. L., Zijdenbos, A. P., Kollokian, V., Sled, J. G., Kabani, N. J., Holmes, C. J., and Evans, A. C. (1998). Design and construction of a realistic digital brain phantom. *IEEE Trans Med Imaging*, 17(3):463–468.
- De Castro, E. and Morandi, C. (1987). Registration of translated and rotated images using finite Fourier transform. *IEEE Trans. Pattern Analysis and Machine Intelligence*, 9(5):700–703.
- Keller, Y., Shkolnisky, Y., and Averbuch, A. (2006). Volume registration using the 3-D pseudopolar Fourier transform. *IEEE Trans. Image Processing*, 54(11):4323–4331.
- Kuglin, C. and Hines, D. (1975). The phase correlation image alignment method. In *Proc. Int. Conf. on Cybernetics and Society*, pages 163–165. IEEE.
- Press, W., Flannery, B., Teukolsky, S., and Vetterling, W. (1992). *Numerical Recipes in C*. Cambridge University Press, second edition.
- Reddy, B. and Chatterji, B. (1996). An fft-based technique for translation, rotation, and scale-invariant image registration. *IEEE Trans. Image Processing*, 5(8):1266–1271.
- Zitová, B. and Flusser, J. (2003). Image registration methods: a survey. *Image and Vision Computing*, 21(11):977–1000.